Metabolism Clinical and Experimental 107 (2020) 154228

Contents lists available at ScienceDirect

Metabolism Clinical and Experimental

journal homepage: www.metabolismjournal.com

PINK1–PRKN mitophagy suppression by mangiferin promotes a brown-fat-phenotype via PKA-p38 MAPK signalling in murine C3H10T1/2 mesenchymal stem cells

Md. Shamim Rahman, Yong-Sik Kim *

Institute of Tissue Regeneration, College of Medicine, Soonchunhyang University, Cheonan, Chung-nam 31151, South Korea
Department of Microbiology, College of Medicine, Soonchunhyang University, Cheonan, Chung-nam 31151, South Korea

ARTICLE INFO

Article history:
Received 29 November 2019
Accepted 7 April 2020
Available online xxxx

Keywords:
Mangiferin
C3H10T1/2
UCP1
PINK1–PRKN mitophagy
Mitochondrial biogenesis
PKA-p38 MAPK-CREB

ABSTRACT

Objective: Mangiferin (MF), a xanthonoid derived from *Mangifera indica*, has shown therapeutic effects on various human diseases including cancer, diabetes, and obesity. Nonetheless, the influence of MF on non-shivering thermogenesis and its underlying mechanism in browning remains unclear. Here, our aim was to investigate the effects of MF on browning and its molecular mechanisms in murine C3H10T1/2 mesenchymal stem cells (MSCs).
Materials/methods: To determine the function of MF on browning, murine C3H10T1/2 MSCs were treated with MF in an adipogenic differentiation cocktail and the thermogenic and correlated metabolic responses were assessed using MF-mediated signalling. Human adipose-derived MSCs were differentiated and treated with MF to confirm its role in thermogenic induction.
Results: MF treatment induced the expression of a brown-fat signature, UCP1, and reduced triglyceride (TG) in C3H10T1/2 MSCs. MF also induced the expression of major thermogenesis regulators: PGC1α, PRDM16, and PPARγ and up-regulated the expression of beiging markers CD137, HSPB7, TBX1, and COX2 in both murine C3H10T1/2 MSCs and human adipose-derived mesenchymal stem cells (hADMSC). We also observed that MF treatment increased the mitochondrial DNA and improved mitochondrial homeostasis by regulating mitofission–fusion plasticity via suppressing PINK1–PRKN-mediated mitophagy. Furthermore, MF treatment improved mitochondrial respiratory function by increasing mitochondrial oxygen consumption and expression of oxidative-phosphorylation (OXPHOS)-related proteins. Chemical-inhibition and gene knockdown experiments revealed that β3-AR-dependent PKA-p38 MAPK-CREB signalling is crucial for MF-mediated brown-fat formation via suppression of mitophagy in C3H10T1/2 MSCs.
Conclusions: MF promotes the brown adipocyte phenotype by suppressing mitophagy, which is regulated by PKA-p38MAPK-CREB signalling in C3H10T1/2 MSCs. Thus, we propose that MF may be a good browning inducer that can ameliorate obesity.

Abbreviations: MF, mangiferin; WAT, white adipose tissue; BAT, brown adipose tissue; hADMSCs, human adipose derived mesenchymal stem cells; UCP1, uncoupling protein 1; PGC1α, peroxisome proliferator-activated receptor gamma coactivator 1-alpha; PRDM16, PR domain containing 16; PPAR, peroxisome proliferator-activated receptor; AP2, adipocyte lipid-binding protein 2; PSAT1, phosphoserine aminotransferase 1; TFAM, mitochondrial transcription factor A; NRF, nuclear respiratory factor; DIO2, iodothyronine deiodinase 2; LCAD, long-chain acyl-CoA dehydrogenases; MCAD, medium-chain acyl-coenzyme A dehydrogenase; LCPT, liposomal carnitine palmitoyltransferase; CPT1α, carnitine palmitoyltransferase I alpha; HSL, hormone-sensitive lipase; ATGL, adipose triglyceride lipase; PLIN, perilipin; β3-AR/ADRB3, beta 3-adrenergic receptor; DGAT2, diacylglycerol O-acyltransferase 2; SREBP1c, sterol regulatory element-binding protein 1; ACC, acetyl-CoA carboxylase; PINK1, PTEN-induced kinase 1; PARKIN/PRKN, Parkin RBR E3 ubiquitin protein ligase; p62, ubiquitin-binding protein p62; LC3B, microtubule-associated proteins 1A/1B light chain 3B; DRP1, dynamin related protein 1; FIS1, mitochondrial fission 1 protein; MFN, mitofusion; OPA1, dynamin-like 120 kDa protein mitochondria; mtDNA, mitochondrial DNA; CD137, cluster of differentiation −137; TBX1, T-box transcription factor TBX1; ZIC1, zinc finger protein ZIC 1; HSPB7, heat shock protein beta-7; COX, cyclooxygenase; CEBP, CCAAT/enhancer-binding protein; FGF21, fibroblast growth factor 21; BMP, bone morphogenetic protein; EBF2, early B cell factor 2; PKA, protein kinase A; p38 MAPK, p38 mitogen-activated protein kinase; CREB, cAMP [cyclic adenosine monophosphate] response element binding protein; AMPK, AMP [adenosine monophosphate]-activated protein kinase; cAMP, adenosine 3′,5′ cyclic monophosphate; ATP, adenosine triphosphate; OXPHOS, oxidative phosphorylation; OCR, oxygen consumption rate; DMEM, Dulbecco's modified Eagle's medium.

* Corresponding author at: Department of Microbiology, College of Medicine, Soonchunhyang University, Soonchunhyang 6 gil 31, Dongnam-Gu, Cheonan, Chung-nam 31151, Republic of Korea.
E-mail address: yongsikkim@sch.ac.kr (Y.-S. Kim).

https://doi.org/10.1016/j.metabol.2020.154228
0026-0495/

1. Introduction

There are two types of fat tissues in adult humans: one is an energy reservoir, white adipose tissue (WAT), and the other is an energy dissipator, brown adipose tissue (BAT). An excess of lipid accumulation in WAT causes obesity that can lead to other health problems such as type II diabetes, cardiovascular diseases, and cancer [1]. BAT burns lipids for heat in a process called non-shivering thermogenesis, which is currently believed to ameliorate obesity. Beige adipose tissue was recently defined as a new adipose tissue type located in subcutaneous WAT that is derived from a distinct cellular lineage in rodents [2]. Brown and beige adipocytes contain multi-locular lipid droplets and strongly express mitochondrial uncoupling protein 1 (UCP1). External cues such as cold exposure and treatment of β3-adrenergic receptor (β3-AR) engagement and PPARγ agonists in WAT can convert the tissue from white to brown adipocyte (browning) and promote white-to-beige transition (beiging), which causes UCP1-dependent heat generation, thereby reducing obesity [3,4].

Multifunctional mitochondrial homeostasis was recently highlighted because its functions and maintenance are directly related to human diseases [5]. Therefore, fine and tight control of mitochondrial biogenesis and degradation are important. Obesity is caused by adipocyte dysfunction following dysregulation of mitochondrial homeostasis including biogenesis, fission-fusion, and mitophagy. In adipocytes, mitochondrial clearance by mitophagy controls the differentiation and promotion of thermogenic signatures [6]. Mitophagy is an autophagic mechanism that occurs specifically in mitochondria. Mitophagy consists of three major steps: 1) fission of the mitochondrial network, 2) priming by autophagy machinery, and 3) engulfment by the autophagosome [7]. Briefly, a changed mitochondrial membrane potential leads to the recruitment of PTEN-induced putative kinase 1 (PINK1) and Parkin, E3 ubiquitin ligase that subsequently polyubiquitinates mitochondrial outer proteins [8,9]. After that, autophagy adaptors, nuclear dot protein 52 kDa (NDP52), optineurin (OPTN), and p62, bind the ubiquitinated proteins to LC3 (microtubule-associated protein 1 light chain 3), leading to the formation of double membraned mitophagosomes [10,11]. The ubiquitin-independent mechanisms that involve BCL2L13 (BCL2 like 13), BNIP3 (BCL2/E1B 19 kDa-interacting protein 3), and FUNDC1 (FUN14 domain-containing protein 1) also can activate mitophagy [12]. It remains under debate whether mitophagy induction promotes differentiation into white adipocytes and beige-to-white trans-differentiation [13]. For the maintenance of beige adipocytes, mitophagy inhibition by a genetic manipulation or pharmacological intervention is required [14]. PINK1–PARKIN (PRKN)-mediated mitophagy in adipose tissue is studied widely [15,16]. It has been reported that β3-AR–dependent PKA and p38 MAPK activations inhibit PINK1–PRKN-mediated mitophagy, thus suppressing beige-to-white reversion [15,17]. In addition, mitophagy suppression preserves a brown-fat signature, which is characterised by high UCP1 expression and mitochondrial biogenesis [18].

Despite efforts made to develop anti-obesity drugs over the past several decades, those that have been developed are limited and new approaches are highly needed. Therefore, browning WAT and activating BAT have become prominent pharmacological strategies for eradicating obesity. Many studies have shown that phytochemicals may be good candidates for anti-obesity drugs because phytochemicals promote the browning of WAT and activation of BAT [19–22]. Researchers have also demonstrated that liensinine and raspberry ketone can inhibit beige-adipocyte reversion to the white phenotype and maintains the beige signature by suppressing mitophagy [23,24]. Nevertheless, there is only limited knowledge about the mechanisms by which phytochemicals activate the brown-fat-like signature and suppress mitophagy. Thus, discovery of potent phytochemicals that can induce the expression of the brown-fat signature and suppress mitophagy has become a popular topic and may lead to a therapeutic method for counteracting obesity.

Mangiferin (MF) from *Mangifera indica* is one of the widely studied phytochemicals owing to its anti-cancer [25], anti-diabetic [26], and anti-obesity [27–29] properties. On the other hand, the impact of MF on the brown-fat-like phenotype remains unclear. In this study, we first demonstrated that the effect of MF on browning is mediated by the suppression of mitophagy in C3H10T1/2 MSCs. Additionally, we investigated the effects of MF on mitochondrial biogenesis and homeostasis, in particular, whether these effects involve modulation of mitofission-fusion plasticity. On the basis of our findings, we can speculate that MF may be a good candidate compound for reducing obesity.

2. Materials and methods

2.1. Materials

Reagents were obtained from the following sources: MF (cat. # M3547), H89, triiodothyronine (T3), insulin, dexamethasone, 3-isobutyl-1-methylxanthine (IBMX), rosiglitazone (Rosi), Oil Red O dye (ORO), 3-(4,5-dimethylthiazol-2-yl)-2,5-diphenyltetrazolium bromide (MTT), 4% formaldehyde, dimethyl sulfoxide (DMSO), and 4′,6-diamidino-2-phenylindole (DAPI) were purchased from Sigma-Aldrich (St. Louis, MO, USA). Carbonyl cyanide p-trifluoro-methoxyphenyl hydrazone (FCCP) was acquired from Cayman Chemicals (Ann Arbor, Michigan, USA). Fetal bovine serum (FBS) and high-glucose Dulbecco's modified Eagle's medium (DMEM/F12) were bought from Atlas Biologicals (Fort Collins, CO, USA), and a penicillin–streptomycin solution was acquired from Hyclone Laboratories, Inc. (South Logan, NY, USA). Antibodies against PGC1α, PRDM16, OXPHOS, PINK1, PARKIN (PRKN), and β3-AR were purchased from Abcam (Cambridge, MA, USA). Antibodies against HSL, ATGL, phospho-(p-)HSL (Ser563 and Ser660), PLIN1, OPA1, aP2, C/EBPβ, AMPK, p-AMPK (Thr172), p38 MAPK, p-p38 MAPK (Thr180/Tyr182), CREB, p-CREB (Ser133), p-PKA substrate, LC3B, and p62 as well as an anti-rabbit IgG (H + L), F(ab′)2 fragment (Alexa Fluor 488 conjugate) antibody, anti-rabbit IgG antibody conjugated with horseradish peroxidase (HRP), anti-mouse IgG antibody conjugated with HRP, and MitoTracker® Red CMXRos were purchased from Cell Signaling Technology (Danvers, MA, USA). Antibodies against UCP1, MFN1, MFN2, DRP1, PPARγ, C/EBPα, and β-actin were bought from Santa Cruz Biotechnology (Dallas, TX, USA). The BCA Protein Assay Kit was acquired from Thermo Scientific (Rockford, IL, USA), and protein loading buffer was bought from Bio-Rad Laboratories, Inc. (Hercules, CA, USA).

2.2. Cell culture, differentiation, and treatment

C3H10T1/2 MSCs (cat. # KCLB-10226) and human adipose-derived MSCs (hADMSCs; ATCC, cat. # PCS-500-011) were cultured in DMEM/F12 GlutaMax supplemented with 10% of FBS and 1% of the penicillin–streptomycin solution in a humidified 5% CO_2 incubator at 37 °C. For adipogenic differentiation, sufficiently confluent C3H10T1/2 cells (passage ≥10; 2 days postconfluence, designated as day 0; Fig. 1B) were incubated with an adipogenic induction cocktail (MDI; 0.5 mM IBMX, 1 μM dexamethasone, and 10 μg/mL insulin) with or without MF in DMEM supplemented with 10% of FBS. Treatments exceeding 2 days were continued until day 4 via replacement of the medium with a solution of MF in the maturation medium consisting of DMEM, insulin (10 μg/mL), and 10% of FBS. From day 4, only the maturation medium was used until cell harvesting. hADMSCs (passage ≤6) were grown to 60–70% confluence (designated as day 0). The cells were then differentiated in DMEM/F12 supplemented with 10 μg/mL transferrin, 1 μM dexamethasone, 500 μM IBMX, 0.85 μM insulin, and 0.2 nM T3. On day 3, IBMX and dexamethasone were not added into the replacement culture medium while 0.5 μM Rosi was added, with culturing until day 9 of differentiation, thereby leading to the development of white hADMSC-derived adipocytes on day 13. To induce the browning program, 40 μM MF was added on day 13 and was present in the medium until day 16. White adipocytes were treated with DMSO from day 13 to day 16. From day 16 to day 23, the differentiation medium of both white and beige adipocytes was free of Rosi.

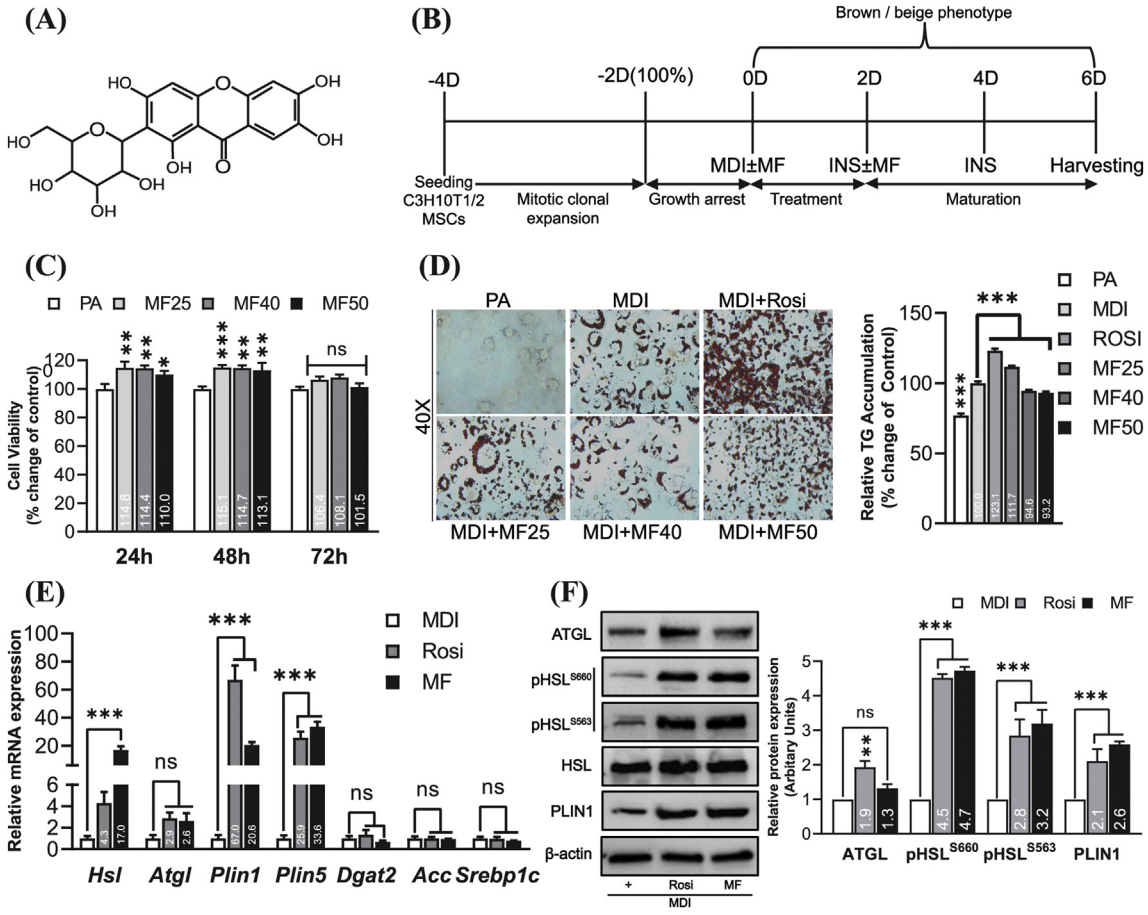

Fig. 1. MF treatment reduces TG accumulation while inducing lipolysis in C3H10T1/2 MSCs. (A) Chemical structure of MF. (B) Schematic illustration of C3H10T1/2 MSCs differentiation. (C and D) Cell viability and intracellular TG accumulation were assessed at three different concentrations of MF (25, 40, and 50 μM) by the MTT assay and ORO staining, respectively. (E and F) mRNA expression and western blot analyses of lipolysis markers and lipogenesis markers. The data are presented as mean ± SEM. Comparisons were performed using analysis of variance (Bonferroni post hoc test). Significant differences between MF-treated C3H10T1/2 cells and MDI-treated and/or untreated (PA) cells are shown as follows: $^{***}P < 0.001$, $^{**}P < 0.01$, $^{*}P < 0.05$, and ns: statistically non-significant. PA: preadipocytes; MDI: 0.5 mM IBMX, 1 μM dexamethasone, and 10 μg/mL insulin; Rosi: rosiglitazone (1 μM); MF25: 25 μM mangiferin; MF40: 40 μM mangiferin; MF50: 50 μM mangiferin.

Throughout the experiment, media were refreshed or changed every other day.

2.3. Cell viability assay

C3H10T1/2 MSCs were seeded in 96-well plates at low density. Next day, 80% to 90% confluent cells were incubated with 25, 40, or 50 μM MF for 24, 48, or 72 h. Then, 20 μL of an MTT (5 mg/mL) solution was added into each well containing 200 μL of the culture medium, and the cells were incubated for 4 h to allow formazan crystal formation at 37 °C. After that, the formazan crystals were dissolved in 150 μL of DMSO, and absorbance was measured at a wavelength of 590 nm on a Victor™ X3 multilabel reader (Perkin Elmer, Waltham, MA, USA).

2.4. ORO staining

C3H10T1/2 MSCs and hADMSCs were differentiated in 6-well plates (for 6 and 23 days, respectively). The matured cells were washed twice with 1× phosphate-buffered saline (PBS), fixed with 10% formalin for 1 h, and stained with a filtered 0.3% ORO solution for 20 min. The stained cells were then rinsed four times with distilled water, and phenotypic changes were photographed using an Axiovert-25 microscope (Carl Zeiss, Jena, Germany). To quantify ORO, the dye was eluted form stained cells with 100% isopropanol, and absorbance was measured at 520 nm on the Victor™ X3 label reader (Perkin Elmer).

2.5. Quantitative RT-PCR (qRT-PCR)

Total RNA from C3H10T1/2 MSCs was extracted by means of the RNA Extraction Kit (Qiagen, Valencia, CA, USA) following the manufacturer's instructions, and cDNA was synthesized from total RNA (1 μg) using the Maxime RT PreMix Kit (Intron Biotechnology, Seoul, Korea) on a Veriti 96-Well Thermal Cycler (Applied Biosystems, Singapore). qRT-PCR was performed on a CFX96™ Real Time PCR (Bio-Rad, Singapore) with the iQTM SYBR Green Supermix Kit (Bio-Rad). The measurement data were normalized to *Tbp* data as a control. Nucleotide sequences of the primers are shown in Supplementary Table 1.

2.6. Western blot analysis

Cells were lysed in RIPA lysis buffer supplemented with protease and phosphatase inhibitors, and total-protein concentration was measured by means of the BCA Protein Assay Kit (Rockford, IL, USA). Protein samples were separated on a sodium dodecyl sulphate 4–20% polyacrylamide gradient gel (Mini-PROTEAN Precast Gel, Bio-Rad) and transferred onto a polyvinylidene difluoride membrane. After that, the membranes were incubated with specific antibodies as indicated in figures. Protein bands were detected by the Chemiluminescent ECL Assay (Advansta, USA) on ChemiDoc™ XRS^{+} with ImageLab (Bio-Rad). The anti-β-actin antibody was employed to set up the loading control.

2.7. Immunofluorescence assay and mitochondrial DNA (mtDNA) content analysis

Cells were differentiated on confocal dishes for 6 days. Then, the cells were incubated with MitoTracker® Red CMXRos (100 nM; Cell Signaling Technology) for 15 min and fixed with ice-cold methanol for 15 min at −20 °C. Following the fixation, the cells were permeabilized with 0.1% Triton X-100 for 15 min and blocked with 1% BSA for 1 h at room temperature. Next, the cells were incubated with the anti-UCP1 (primary) antibody (Abcam) overnight at 4 °C followed by the Alexa Fluor 488–conjugated anti-rabbit IgG (secondary) antibody (Cell Signaling Technology) for 1 h at room temperature. Cell DNA was stained with 1 μg/mL DAPI for 1 min at room temperature, and images were captured with a confocal microscope (Olympus Fluoview FV10i; Tokyo, Japan) in a fluorescent mounting medium containing an antifading agent (Dako, CA, USA). MtDNA content was evaluated by qRT-PCR analysis of a mitochondrial gene, cytochrome *c* oxidase subunit I (*CoxI*); these data were normalized to the expression of a nuclear ribosomal protein gene, *p0*, as described elsewhere [30].

2.8. PKAα and p38 MAPKα knockdowns

C3H10T1/2 MSCs were cultured in 6-well plates and allowed to grow up to 80–90% confluence. Then, the cells were transfected with control siRNA (siCont, 100 pM), PKAα siRNA (siPKA, 100 pM), or p38 MAPKα siRNA (sip38, 100 pM) oligonucleotide duplexes (Santa Cruz Biotechnology, Inc.) via 6 μL/well Lipofectamine 2000 (Invitrogen, Carlsbad, CA) according to the manufacturer's instructions. The transfection efficiency was determined by qRT-PCR and western blotting.

2.9. Oxygen consumption assay

C3H10T1/2 MSCs were seeded in a 96-well plate at 4–6 × 10^4 cells/well and differentiated for 6 days. The oxygen consumption rate (OCR) was determined by means of the Oxygen Consumption Assay Kit (Cayman Chemicals, USA) according to the manufacturer's instructions. The positive-control samples were incubated with glucose oxidase (Gox) or mitochondrial OXPHOS uncoupler FCCP, and negative control samples with antimycin A (complex III inhibitor). The fluorescence was measured at excitation and emission wavelengths of 380 and 650 nm, respectively, on the Victor™ X3 multilabel plate reader (Perkin Elmer). All the samples were compared with adipogenic differentiation medium (MDI)-treated cells.

2.10. Mitophagy assay

To assess mitophagy flux, PINK1–PRKN-mediated mitophagy was induced by FCCP (10 μM) in C3H10T1/2 MSCs [31]. Mitophagy was detected in MF- and/or FCCP-treated cells by staining with Mtphagy (100 nM) and Lyso Dye® (1 μM), respectively, for 30 min at 37 °C from the Mitophagy Detection Kit (Dojindo Molecular Technologies, Rockville, USA) according to the manufacturer's instructions. Following a DMEM wash, fluorescence images were captured with the confocal microscope (Olympus Fluoview FV10i; Tokyo, Japan).

2.11. Densitometry in the ImageJ software

The western-blot images and immunofluorescence-staining images were quantitatively analyzed in the ImageJ software (NIH, Bethesda, MD, USA) as described previously [32]. Before the quantification, the immunofluorescence images were converted to a weighted 8-bit grayscale format and then inverted.

2.12. Statistical analysis

All values were expressed as mean ± standard error of the mean (SEM). The experimental variables were confirmed with at least triplicate biological samples. Depending on the experiments, one- or two-way ANOVA with the post hoc Bonferroni test was carried out to determine the significance of differences based on probability <0.05, <0.01, <0.001, and ≥ 0.05 (not significant). All the statistical analyses were performed in GraphPad Prism 8 (GraphPad Software, La Jolla, CA, USA).

3. Results

3.1. MF reduces TG accumulation but induces lipolysis in C3H10T1/2 MSCs

To determine the treatment dose of MF, we measured cell viability at three doses of MF (25, 40, and 50 μM) applied to C3H10T1/2 MSCs and hADMSCs. As shown in Fig. 1C, none of the MF doses had any toxic effect on C3H10T1/2 MSCs at 24, 48, and 72 h. Nevertheless, among hADMSCs, the number of viable cells slightly diminished (Supplementary Fig. 4B); a similar observation about hADMSCs has been reported previously [29]. Besides, we determined the influence of MF on intracellular TG accumulation. As presented in Fig. 1D, 40 and 50 μM MF-treated cells accumulated less TGs, whereas 25 μM MF-treated cells and Rosi-treated cells accumulated more TGs. Of note, 40 μM MF treatment has been proven to inhibit adipogenesis in hADMSCs [29]. Therefore, we selected 40 μM MF for further analyses. Next, the data on the reduction in TG accumulation allowed us to investigate whether MF affects lipolysis. Therefore, we tested the expression of lipolytic markers in MF-treated cells in comparison with MDI (negative control)-treated cells and Rosi (positive control)-treated cells. As depicted in Fig. 1E, MF increased mRNA levels of initial-stage lipolytic gene *Atgl* up to 2.6-fold and of *Hsl* (a final-stage lipolysis gene) more significantly: 17.0-fold. In addition, the expression of other lipolytic genes such as *Plin1* (20.6-fold) and *Plin5* (33.6-fold) was significantly increased by MF. By contrast, MF treatment severely reduced the expression of several lipogenesis genes: *Dgat2* (~0.1-fold), *Srebp1c* (~0.3-fold), and *Acc* (~0.4-fold). The lipolytic proteins were also coherently changed with mRNA expression. The expression of lipolytic proteins ATGL (1.3-fold), $pHSL^{S563}$ (3.2-fold), $pHSL^{S660}$ (4.7-fold), and PLIN1 (2.6-fold) was highly enhanced by MF (Fig. 1F). These data indicate that MF improves the intracellular lipid profile by activation of lipolytic genes and via suppression of lipogenic genes in C3H10T1/2 MSCs.

3.2. MF induces brown-fat phenotype and browning in C3H10T1/2 MSCs

To understand the stimulatory effect of MF on the brown-fat phenotype, we tested the expression of beige markers in 40 μM MF-treated C3H10T1/2 MSCs. As illustrated in Fig. 2A, MF treatment increased the mRNA expression of beige-fat-specific markers *Cd137* (10.7-fold), *Tbx1* (4.1-fold), *Zic1* (13.0-fold), *Hspb7* (27.1-fold), and *Fgf21* (29.3-fold) and of brown-fat–specific markers *Cox2* (4.3-fold) and *Cox1* (2.4-fold). Additionally, *Cd137* (3.3-fold) and *Tbx1* (6.0-fold) mRNA levels were up-regulated in hADMSCs by MF treatment (Fig. 2B). MF treatment also significantly raised the expression of genes *Ebf2* (4.3-fold), *Bmp4* (3.8-fold), and *Bmp7* (6.4-fold), which are known to perform critical functions in early beige-lineage development (Fig. 2A and C). Moreover, we checked the expression of other lineage markers during adipocyte development (Supplementary Fig. 1) and tested the expression of common adipogenic-commitment markers in the MF-treated cells. MF treatment enhanced the expression of early marker *Cebpβ* (54.2-fold) and of late marker *Cebpα* (2.9-fold; Fig. 2D). Additionally, MF raised the protein expression of CEBPβ (2.3-fold) and CEBPα (1.5-fold) while significantly reducing the expression of white-fat-specific protein AP2 (0.5-fold; Fig. 2G). Nonetheless, it is noteworthy that the

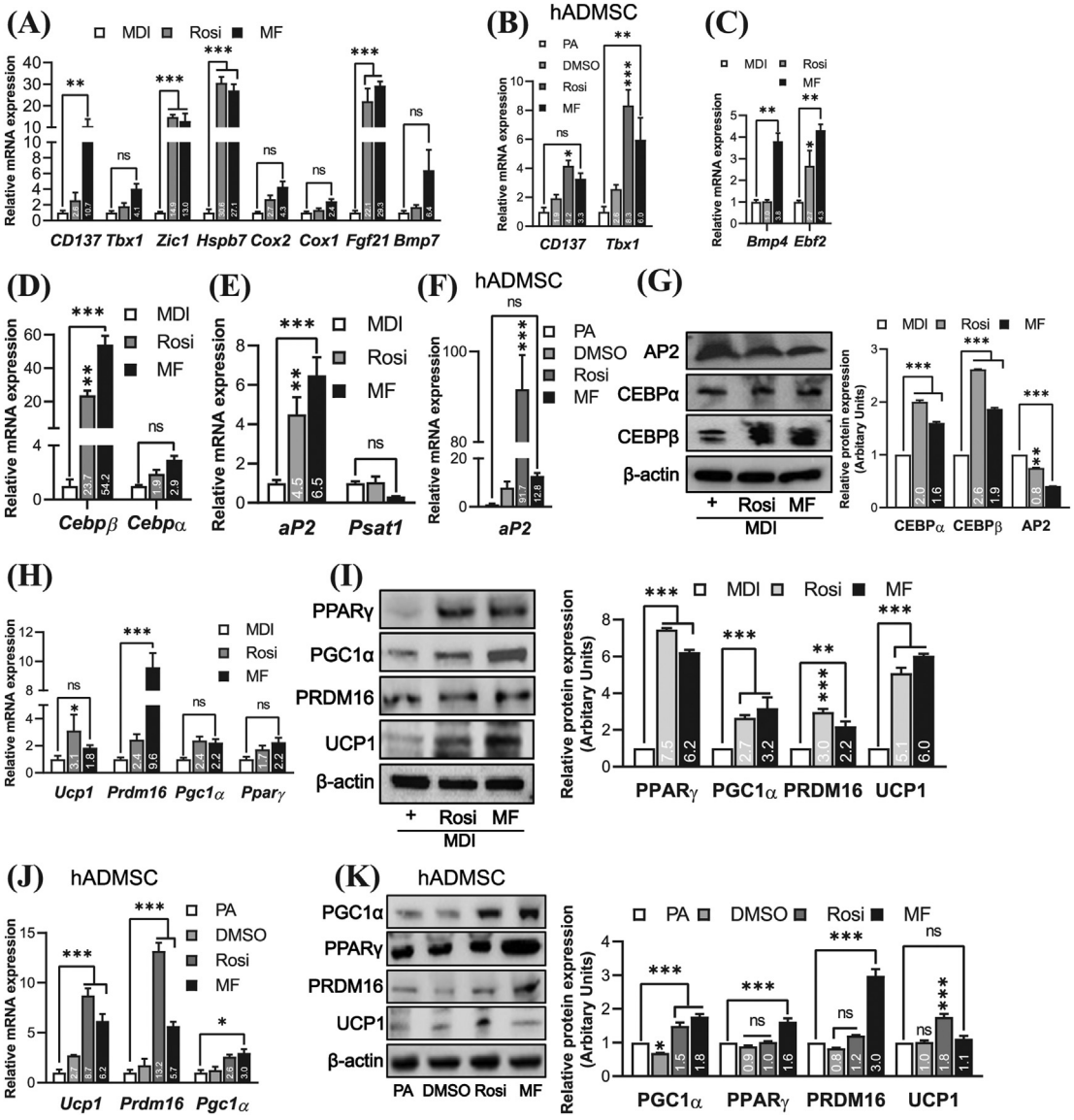

Fig. 2. MF treatment alters the expression of white-, beige-, and brown-fat-related genes in differentiated C3H10T1/2 cells and hADMSCs. (A and B) Expression of beige-fat-specific genes (*Cd137*, *Tbx1*, *Zic1*, *Hspb7*, *Cox2*, *Cox1*, *Fgf21*, and *Bmp7*) in C3H10T1/2 cells and hADMSCs, respectively. (C and D) mRNA expression of early beige- and/or brown-commitment markers and adipogenic-commitment markers, respectively. (E and F) mRNA levels of white-fat markers in C3H10T1/2 and hADMSCs, respectively. (G) The expression of common white- and adipogenic-commitment markers (proteins AP2, CEBPβ, and CEBPα) in MF-treated C3H10T1/2 MSCs. Expression of common thermogenic markers (*Ucp1*, *Prdm16*, *Pgc1α*, and *Pparγ*) in C3H10T1/2 cells (H, I) and in hADMSCs (J, K). The data are presented as mean ± SEM. Comparisons were performed with analysis of variance (Bonferroni post hoc test). The significance of differences between MF-treated C3H10T1/2 cells and MDI-treated and/or untreated (PA) cells is depicted as follows: $^{***}P < 0.001$, $^{**}P < 0.01$, $^{*}P < 0.05$, and ns: statistically non-significant. PA: preadipocytes; MDI: 0.5 mM IBMX, 1 μM dexamethasone, and 10 μg/mL insulin; Rosi: rosiglitazone; DMSO: dimethyl sulphoxide; MF: 40 μM mangiferin.

expression of late-stage white-fat-specific marker *aP2* increased in both the Rosi-treated group and MF-treated group while the expression of *Psat1* significantly diminished in both groups (Fig. 2E and F). Finally, we measured the expression of common thermogenic markers both in C3H10T1/2 cells and hADMSCs. In C3H10T1/2 cells, MF treatment enhanced the mRNA expression of *Ucp1* (1.8-fold), *Pgc1α* (2.2-fold), *Pparγ* (2.2-fold), and *Prdm16* (9.6-fold; Fig. 2H). Similarly to mRNA expression, the protein levels of UCP1 (6.0-fold), PGC1α (3.2-fold), PPARγ (6.2-fold), and PRDM16 (2.2-fold) were increased by the treatment with MF (Fig. 2I). We also confirmed the mRNA up-regulation of *Ucp1* (6.2-fold), *Pgc1α* (3.0-fold), and *Prdm16* (5.7-fold) and protein up-regulation of UCP1 (1.1-fold), PGC1α (1.8-fold), PPARγ (1.6-fold), and PRDM16 (3.0-fold) in MF-treated hADMSCs (Fig. 2J and K). These results suggest that MF can induce thermogenesis in both C3H10T1/2 and hADMSCs.

3.3. MF promotes mitochondrial β-oxidation, biogenesis, and OXPHOS

Previously, we have demonstrated that MF induces lipolysis-related genes thus leading to the formation of free fatty acids. It is known that free fatty acids are utilised by mitochondrial β-oxidation for ATP production. Mitochondrial β-oxidation acts as an energy source for mitochondrial biogenesis, which is the key contributor to thermogenesis. Accordingly, we investigated the influence of MF on the mitochondrial functions. We evaluated the expression of mitochondrial β-oxidation markers. MF treatment significantly increased the expression of β-oxidation-related genes including *Lcad* (8.8-fold), *Mcad* (23.1-fold), *Cpt1α* (3.8-fold), *Lcpt* (67.6-fold), and *Pparα* (2.4-fold; Fig. 3A). Then, we measured the expression of mitochondrial biogenesis genes in MF-treated C3H10T1/2 cells. MF treatment significantly increased the expression of *Dio2*

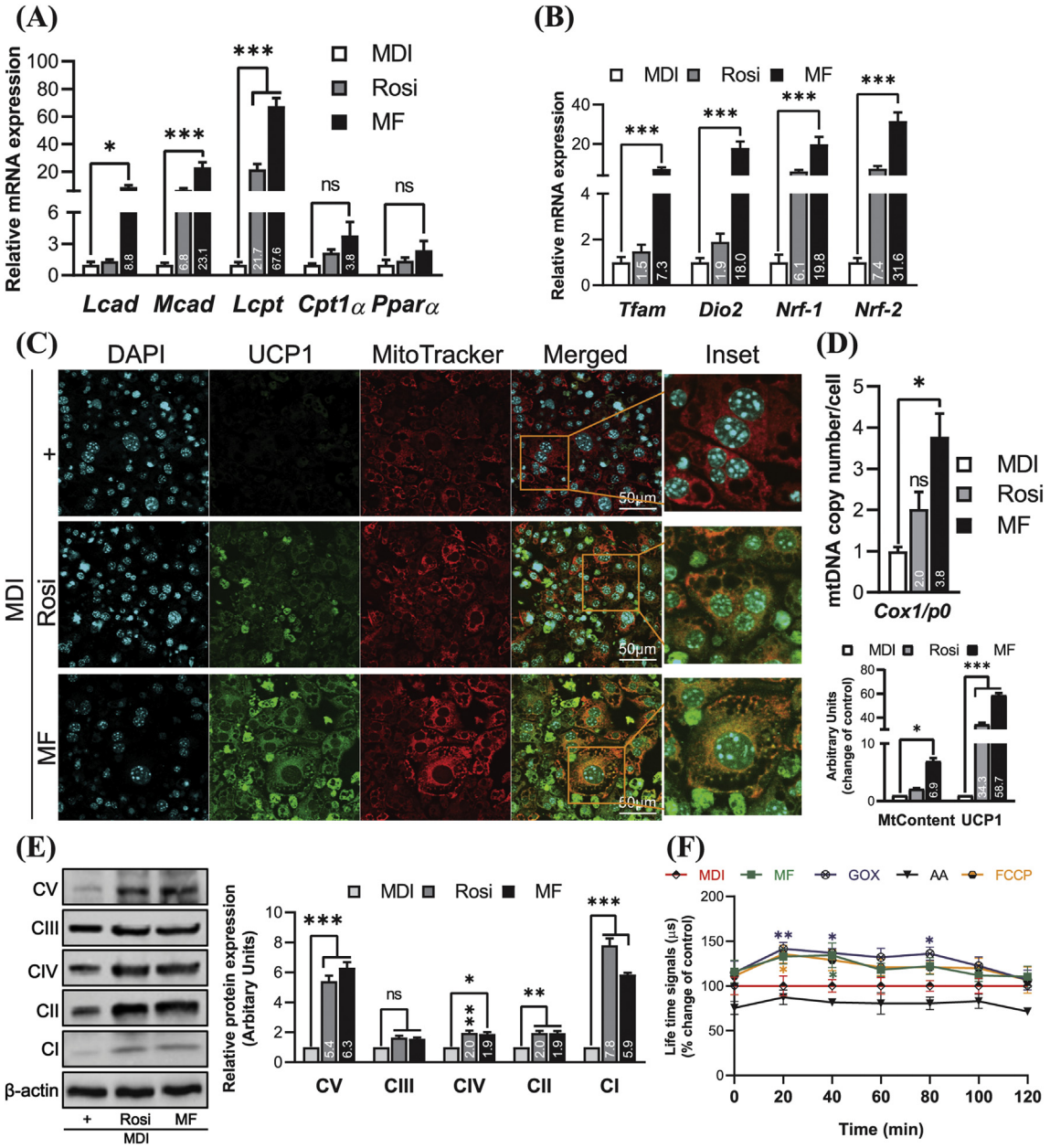

Fig. 3. MF treatment improves mitochondrial biogenesis and respiration in C3H10T1/2 MSCs. mRNA expression levels of mitochondrial lipid β-oxidation–related genes (A) and mitochondrial biogenesis markers (B). (C) Immunofluorescence analysis of UCP1 and MitoTracker, and quantification of mitochondrial content of cells (MitoTracker) and UCP1 expression according to ImageJ densitometry. (D) mRNA levels of a mitochondrial gene, *Cox1*, compared to the *P0* gene. (E) Expression and quantification of OXPHOS complexes I–V (CI–CV). (F) The OCR (≥120 min) during the treatment of C3H10T1/2 MSCs with MF, where GOX and FCCP represent a positive control, antimycin A (AA) is a negative control, and MDI treatment served as the baseline control. The data are expressed as mean ± SEM. Comparisons were performed with analysis of variance (Bonferroni post hoc test). Significant differences between MF-treated C3H10T1/2 cells and MDI-treated cells are shown as follows: $^{***}P < 0.001$, $^{**}P < 0.01$, $^{*}P < 0.05$, and ns: statistically non-significant. MDI: 0.5 mM IBMX, 1 μM dexamethasone, and 10 μg/mL insulin; Rosi: rosiglitazone; MF: 40 μM mangiferin; Gox: glucose oxidase; AA: antimycin A; FCCP: a mitochondrial OXPHOS uncoupler.

(18.0-fold), *Tfam* (7.3-fold), *Nrf1* (19.8-fold), and *Nrf2* (31.6-fold; Fig. 3B). Increased mitochondrial biogenesis results in high expression of mitochondrial UCP1. Immunostaining images also indicated that MF treatment significantly increased mitochondrial mass and UCP1 expression as compared to the control groups: MDI and Rosi (Fig. 3C). Additionally, the quantitative analysis of mtDNA showed that MF treatment increased the mtDNA copy number in C3H10T1/2 MSCs (Fig. 3D). Next, we estimated mitochondrial respiration in MF-treated cells. As presented in Fig. 3E, MF treatment significantly increased total expression of OXPHOS proteins (complexes I–V). Although the spatial assembly of OXPHOS complexes in the mitochondrial membrane is not clear, it is known that OXPHOS complexes (I–IV) are inserted into the mitochondrial inner membrane, whereas complex V (ATPase) into mitochondrial cristae. Except for complex II, all the OXPHOS complexes contain at least one mtDNA-encoded subunit. OXPHOS directly contributes to ATP production via ATP synthase (complex V). Furthermore, we found that the oxygen consumption rate (OCR) rose until approximately minute 120 in MF-treated cells (Fig. 3F). These data led us to assume that the high OCR coupled with the rapid ATP production via OXPHOS were caused by MF treatment. Overall, MF treatment of C3H10T1/2 MSCs promotes mitochondrial respiration and subsequent thermogenesis.

3.4. MF maintains mitofission-fusion plasticity and suppresses mitophagy

The regulation of mitochondrial homeostasis controls the whole thermogenesis process in adipose tissues. Mitochondrial fission and fusion dynamics require tight regulation, and an imbalance of this plasticity causes mitophagy. Recently, researchers demonstrated that the induction of mitophagy leads to differentiation into white adipocytes and promotes beige-to-white transition. To understand the influence of MF on mitochondrial homeostasis, firstly, we investigated the expression of mitofission- and fusion-related genes. MF treatment significantly raised the mRNA expression of *Mfn1* (7.3-fold), *Mfn2* (17.4-fold), *Opa1* (3.8-fold), *Drp1* (11.9-fold), and *Fis1* (11.9-fold; Fig. 4A). Accordingly, MF also enhanced the expression of proteins MFN1 (3.7-fold), MFN2 (6.4-fold), OPA1 (1.9-fold), and DRP1 (6.5-fold; Fig. 4B). After that, we evaluated the expression of mitophagy-specific markers. MF treatment reduced the expression of *Pink1* (~0.1-fold) and *Prkn* (~0.6-fold) but enhanced the expression of *p62* (lysosome-degrading protein gene) significantly, up to 10.2-fold (Fig. 4C). Accordingly, PINK1 (~0.3-fold), PRKN (~0.6-fold), and LC3B (~0.6-fold) protein levels were reduced but the p62 amount (3.1-fold) was increased by MF in C3H10T1/2 MSCs (Fig. 4D). These findings prompted us to hypothesise that MF might help to balance mitofission and fusion, which in turn maintain mitochondrial membrane potential at the optimal level that results in the suppression of PINK1–PRKN-mediated mitophagy. Mitophagy suppression was confirmed too, by means of the Mtphagy dye, in FCCP-treated C3H10T1/2 MSCs and FCCP-and-MF-co-treated C3H10T1/2 MSCs. MF treatment inhibited mitophagy as seen in confocal-microscopy images (Fig. 4E). Taken together, these findings suggest that MF treatment can increase mitochondrial mass by down-regulating mitophagy in C3H10T1/2 MSCs.

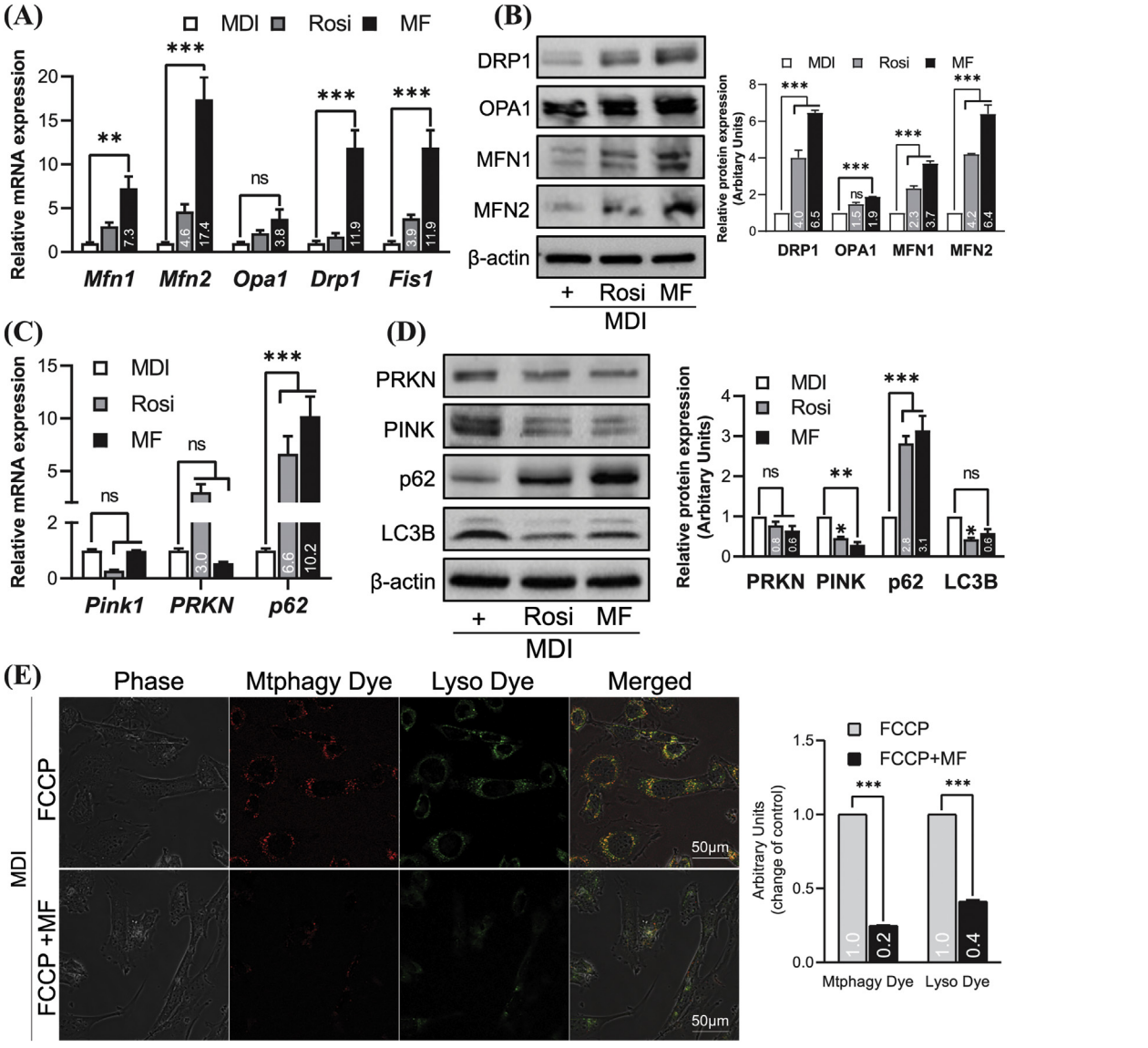

Fig. 4. MF treatment regulates mitochondrial fission-fusion plasticity and suppresses PINK1–PRKN-mediated mitophagy in C3H10T1/2 MSCs. (A) mRNA levels of mitochondrial fission- and fusion-related genes. (B) Expression of fission- and fusion-related proteins (OPA1, DRP1, MFN1, and MFN2). (C) Expression of genes (*Pink1*, *Prkn*, and *p62*) related to PINK1–PRKN-mediated mitophagy. (D) Western blot analysis of mitophagy-related proteins (PINK1, PRKN, p62, and LC3B). (E) The fluorescence images of mitophagy caused by FCCP. Images of FCCP-and-MF-treated cells are presented too. For detection of mitophagy, the cells were treated with either 10 μm FCCP or with 10 μm FCCP and 40 μM MF for 18 h. The data are displayed as mean ± SEM. Comparisons were performed with analysis of variance (Bonferroni post hoc test). The significance of differences between MF-treated C3H10T1/2 cells and MDI-treated ones is illustrated as follows: $^{***}P < 0.001$, $^{**}P < 0.01$, $^{*}P < 0.05$, and ns: statistically non-significant.

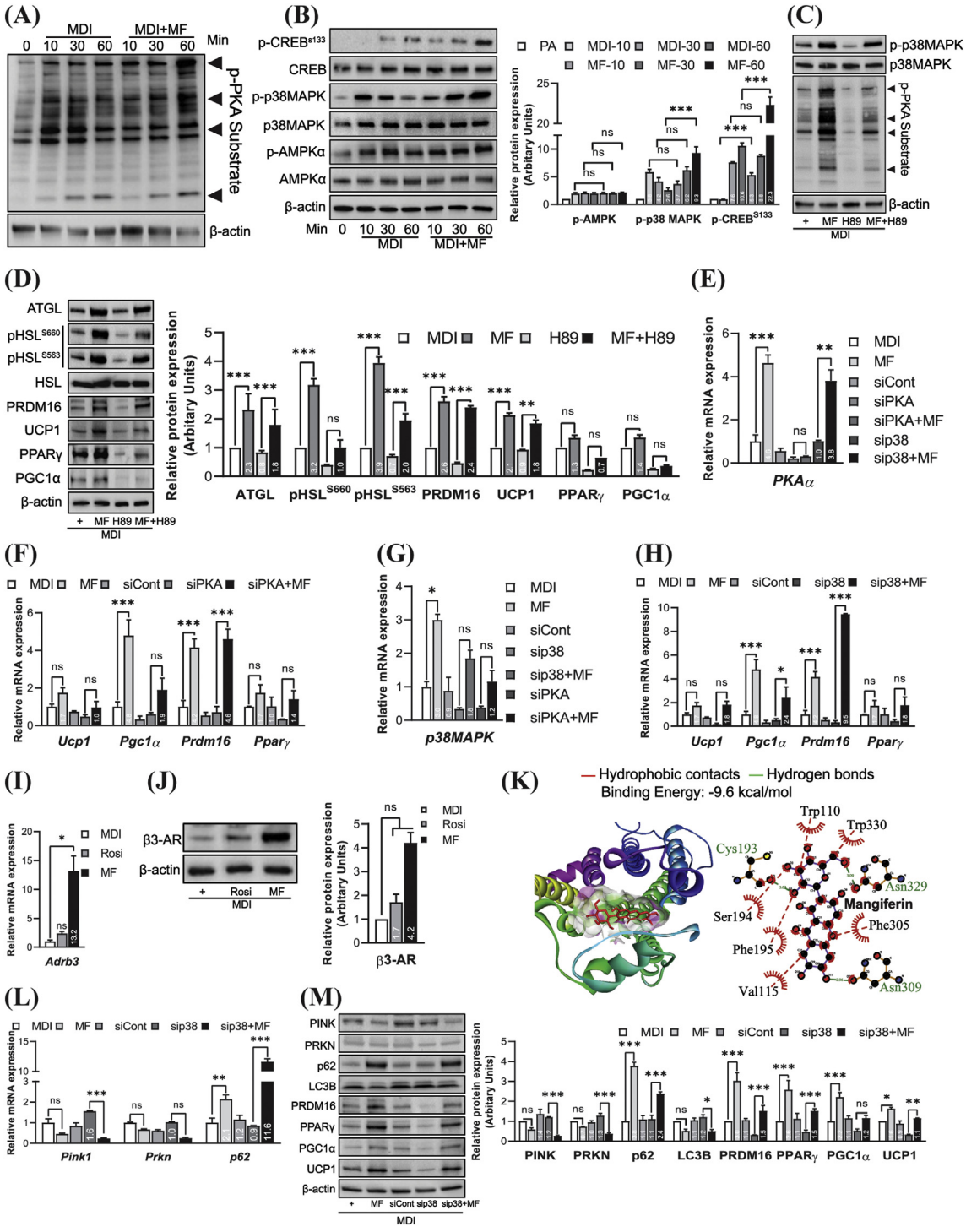

Fig. 5. MF induces browning and suppress PINK1–PRKN-mediated mitophagy by activating β3-AR-dependent PKA–p38 MAPK–CREB signalling in C3H10T1/2 MSCs. (A) Phosphorylation of PKA induced by MF treatment for various periods (10, 30, and 60 min). (B) Phosphorylation of the downstream proteins of PKA signalling, i.e. p38 MAPK and CREB, during thermogenesis induced by MF treatment for various periods (10, 30, and 60 min). For detection of phosphorylated proteins, confluent C3H10T1/2 MSCs were serum starved for 8 h and then incubated with MF for the indicated periods. (C and D) Phosphorylation of PKA and the amounts of PKA target proteins p38 MAPK and p-p38 MAPK and of thermogenic markers (UCP1, PGC1α, PRDM16, PPARγ, pHSL, and ATGL), respectively, under the influence of a pan-PKA inhibitor, H89. (E) *Pkaα* mRNA expression after the siRNA (siPKA) knockdown of PKAα, the knockdown of p38 MAPKα (the sip38 group), the knockdown of PKAα (the siPKA group) together with 40 μM MF treatment (the siPKA + MF group), and the knockdown of p38 MAPKα together with 40 μM MF treatment (group sip38 + MF). siCont stands for the negative control siRNA. (F) The expression of PKAα target thermogenic genes *Ucp1*, *Pgc1α*, *Prdm16*, and *Pparγ* after the knockdown of PKAα (by siPKA). (G) p38 MAPKα mRNA expression in groups sip38, siPKA, si38 + MF, and siPKA + MF. (H) mRNA expression of p38 MAPKα downstream genes (*Ucp1*, *Pgc1α*, *Prdm16*, and *Pparγ* during thermogenesis. (I and J) The mRNA and protein expression levels of β3-AR during treatment with MF. (K) Molecular docking analysis representing the MF interaction with β3-AR. For detailed information, see Supplementary materials. (L) Expression of mitophagy-related genes, *Pink1*, *Prkn*, and *p62*, after the knockdown of p38 MAPK (i.e. in sip38-transfected cells). (M) Western blot analysis of thermogenic markers (UCP1, PGC1α, PRDM16, and PPARγ) and mitophagy markers (PINK1, PRKN, p62, and LC3B) after the knockdown of p38 MAPK. The data are presented as mean ± SEM. Comparisons were performed with analysis of variance (Bonferroni post hoc test). Significant differences between MF-treated C3H10T1/2 cells and MDI-treated and/or untreated (PA) cells are indicated as follows: $^{***}P < 0.001$, $^{**}P < 0.01$, $^{*}P < 0.05$, and ns: statistically non-significant.

3.5. MF activates β3-AR-dependent PKA–p38 MAPK–CREB signalling during promotion of browning and maintenance of mitochondrial homeostatic plasticity in C3H10T1/2 MSCs

To elucidate the mechanism of action of MF on the brown-fat signature and mitochondrial homeostasis, we investigated PKA, CREB, and p38 MAPK signalling. Firstly, we tested PKA phosphorylation after MF treatment. As depicted in Fig. 5A, PKA phosphorylation significantly increased after 60 min of MF treatment as compared to MDI treatment. Next, we measured the signalling downstream of PKA. We observed that MF treatment increased phosphorylation of p38 MAPK and $CREB^{S133}$ too, up to ~9.3- and ~22.3-fold, respectively, while AMPKα phosphorylation was not affected (Fig. 5B). A chemical inhibition assay based on H89 (10 μM), a pan-PKA inhibitor, revealed that the phosphorylation of PKA decreased after H89 treatment, whereas co-treatment with MF recovered the phosphorylation of PKA and p38 MAPK; in addition, PKA inhibition reduced p38 MAPK expression, suggesting that PKA may be upstream of p38 MAPK (Fig. 5C). Then, we evaluated the expression of lipolytic and thermogenic proteins downstream of PKA in MF-and-H89-co-treated cells. We found that co-treatment with MF recovered the expression of ATGL (1.8-fold), $pHSL^{S660}$ (1.0-fold), $pHSL^{S563}$ (2.0-fold), UCP1 (1.8-fold), PGC1α (0.4-fold), PPARγ (0.7-fold), and PRDM16 (2.4-fold) that was inhibited by H89 alone (Fig. 5D). To confirm that PKA or p38 MAPK signalling contributes to MF-induced browning, we implemented a knockdown of PKAα or p38 MAPKα by the siRNA method. In PKAα knockdown cells, *Pkaα* mRNA expression diminished by ~80%, whereas MF treatment recovered the expression of *Pkaα* mRNA slightly. By contrast, in p38 MAPKα knockdown cells, *Pkaα* mRNA expression was unaffected, but MF treatment strongly increased it (Fig. 5E). To further characterise the signalling downstream of PKA during browning, we assessed the expression of thermogenic genes in PKAα knockdown cells. As illustrated in Fig. 5F, the mRNA expression of *Ucp1*, *Pgc1α*, *Pparγ*, and *Prdm16* was significantly reduced by siPKA (by ~60%, ~40%, ~30%, and ~70%, respectively). In contrast, co-treatment with MF recovered these expression levels (Fig. 5F). To confirm that p38 MAPKα is downstream of PKAα, we implemented a knockdown of p38 MAPKα by siRNA. We observed that *p38 MAPKα* mRNA expression was reduced by 70% by sip38 and by roughly the same percentage by siPKA treatment too. Nevertheless, the expression of p38 MAPKα and its downstream gene expressions were recovered by MF co-treatment, suggesting that PKAα is upstream of p38 MAPKα (Fig. 5G and H). In addition, as shown in Fig. 5I and J, the expression of β3-AR increased in MF-treated cells. Consequently, we hypothesised that MF exerts its actions in a β3-AR-dependent manner. In silico molecular docking analysis indicated that MF interacts with residues Ser^{194}, Val^{115}, Trp^{330}, Trp^{110}, Phe^{305}, Asn^{309}, Cys^{193}, Asn^{329}, and Phe^{195} on the β3-AR surface similarly to the interactions involving noradrenaline, CL316,243, or SDG (Fig. 5K) [33]. Our results suggested that MF may act as an agonist of β3-AR through β3-AR–PKA–p38 MAPK signalling. Furthermore, we investigated p38 MAPKα signalling during mitophagy suppression. We observed that PINK1–PRKN-mediated mitophagy was up-regulated by the p38 MAPKα knockdown, but MF co-treatment reduced the expression of PINK1, PRKN, and LC3B and induced p62 and common thermogenic markers significantly (Fig. 5L and M). These data suggest that MF stimulates β3-AR-dependent PKA–p38 MAPK–CREB signalling and enhances the brown-fat-like signature via down-regulation of PINK1–PRKN-mediated mitophagy in C3H10T1/2 MSCs.

4. Discussion

Inappropriate mitofission–fusion leads to mitochondrial damage that requires removal by mitophagic processing unless the mitochondrial membrane potential remains at the optimal level. Mitofission–fusion activation reportedly induces a thermogenic signature because elongated mitochondria are spared from autophagic degradation to maintain ATP levels [34]. Mitochondrial fission is a general process that is crucial for mitophagy. GTPase dynamin-related protein 1 (Drp1) plays important roles in mitochondrial dynamic and mitophagy. Researchers demonstrated that Drp1 can bind to mitochondrial fusion factor OPA1 and that AMPK phosphorylation increases Drp1 recruitment and leads to fission [35]. However, interestingly, another group showed that absence of Drp1 can promote mitophagy, while the absence of Mfn1 and Mfn2 can inhibit mitophagy [36]. This is in line with previous findings in which rosiglitazone- and GW7647-induced beige signatures from hADMSCs showed higher mitofission–fusion-related gene expression [37]. In this study, MF treatment enhanced the expression of mitofusion-related genes such as *MFN1*, *MFN2*, and *OPA1* and mitofission-related genes *DRP1* and *FIS1* [37]. Hence, we speculated that MF may suppress mitophagy by balancing mitofission–fusion. It is also worth mentioning that p38 MAPK inhibition increases Drp1 while downregulating Mfn2 expression (supplementary information), suggesting that PKA inhibition can promote mitophagy by inducing Drp1 and reducing Mfn2 level. As we found, *p38 MAPK* remains downstream of *PKA* in β3-AR-dependent promotion of thermogenesis in adipocytes, which is supported by a previous study [38]. However, little is known about how mitofission–fusion controls mitochondrial depolarization, in turn suppressing mitophagy; thus, further studies are required to reveal this phenomenon.

Kajimura S. et al. have demonstrated that autophagy-induced mitochondrial homeostasis is crucial for beige-cell maintenance [13,14]. Furthermore, PINK1–PRKN-mediated mitophagy has an important role in mitochondrial homeostasis in beige adipocytes [15,16]. However, it is noteworthy that in vivo mitophagy is mostly tissue specific and depends on tissue stress and the underlying signalling pathway. The PINK1/PRKN may not be the only major regulatory pathway of in vivo basal mitophagy [39,40]. For instance, β3-AR agonist CL 316,243 treatment in subcutaneous inguinal WAT strongly induces UCP1 by decreasing parkin expression, whereas parkin expression was unchanged in gonadal WAT but UCP1 was weakly induced in mice [41]. In addition, PRKN-deficient mice showed strong induction of UCP1 expression in the gonadal WAT, suggesting that PRKN may show blunted browning response in gWAT and sWAT [41]. Another study showed that CL316,243-treated PRKN-deficient mice do not have different numbers or distributions of UCP1-positive multilocular beige adipocytes compared to control mice, suggesting that PRKN is not required for beige adipocyte biogenesis [15]. Otherwise, cold-exposed PINK1-deficient mice showed mitochondrial defects in BAT [42] that were not observed in cold-exposed PRKN-deficient mice [15,43,44]. These findings suggest that alternative mechanisms downstream of PINK1 control mitochondria quality in the absence of PRKN [10]. Taken together, PINK1/PRKN function is highly tissue specific and its function may be unnecessary in wild-type and PINK1/PRKN deficient mice, even though it may differ between fat deposits in same animals. However, the intraperitoneal injection (IP) of MF into PINK1/PRKN-deficient mice can help us understand the mechanism of MF-mediated browning and inhibition of beige to WAT transition via suppressing PINK1/PRKN-mediated mitophagy. Thus, extensive researches focusing on MF treatments in PINK1/PRKN-deficient mice are inevitable for exploring the in vivo effects of MF on mitophagy.

In the mitophagic process, LC3B serves as a substrate that is present in autophagosomal membranes and serves as a key marker of autophagosome formation. Mitochondrial recruitment to autophagosomes may occur in an adaptor-dependent or -independent manner. High expression of the adaptor p62 is known to degrade autophagosome and improve mitochondrial function and thermogenesis via β-adrenergically mediated p38 MAPK signalling [45]. During β3-AR stimulation, p38 MAPK knockdown led to mitophagy, whereas p38 MAPK phosphorylation inhibited mitophagy in adipocytes, suggesting that p38 MAPK is crucial for mitophagy [17]. In this study, MF treatment reduced LC3B expression, suggesting that the mitophagy suppression

caused by MF may be mediated by an LC3B pathway. We noted that MF can increase p62 expression, and our siRNA knockdown and chemical inhibition experiments revealed that mitophagy inhibition is regulated by PKA–p38 MAPK signalling. Our findings are supported by other studies, where cAMP signalling repressed autophagy via activation of PKA and p38 MAPK signalling [46].

Scientists found that the repression of autophagy improves the intracellular lipid profile, mitochondrial oxygen consumption, and the expression of OXPHOS and thermogenic genes such as *UCP1*, *DIO2*, and *PPARα* in BAT [46]. In line with these observations, we found that MF treatment can induce phosphorylation of PKA and p38 MAPK instead of AMPK and promote mitochondrial respiration and expression of OXPHOS proteins in C3H10T1/2 MSCs. Thus, we can speculate that the alteration of mitochondrial mitofission–fusion-related genes induced by MF treatment led to improved mitochondrial homeostasis and function in C3H10T1/2 MSCs.

MF has also been reported to induce *Pgc1α*, the core regulator of mitochondrial biogenesis, which positively correlates with the mtDNA amount, as seen with the doubled mtDNA amount in high-fat diet–fed mice [47]. MF improves the lipid profile and mitochondrial bioenergetics via induction of *Pgc1α*, *Pparα*, *Lpl*, *Cpt1*, and *Tfam* and suppression of lipogenesis via down-regulation of *Srebp1c* [48,49]. Lipid β-oxidation contributes to mitochondrial biogenesis and respiration [50,51]. It is noteworthy that MF improves mitochondrial capacity and thermogenesis by raising OCR and carbohydrate oxidation [52]. MF helps to sustain mitochondrial membrane potential and to reduce reactive oxygen species production in hypercholesterolemic mice [53]. We demonstrated that MF promotes mitochondrial biogenesis and enhances oxidative metabolism, resulting in increased production of energy, namely, ATP. MF treatment increased the expression of known regulators of mitochondrial biogenesis TFAM, DIO2, NRF1, and NRF2. Consequently, MF treatment enhanced mitochondrial OCR and the expression of OXPHOS proteins and UCP1. Moreover, we found that MF treatment significantly increases the expression of adipogenic genes including *C/EPBβ*, *EBF2*, *FGF21*, and *PGC1α*. It is known that EBF2 is a key early commitment marker of browning and can cause the recruitment of beige adipocytes into WAT when they are incubated with a β3-AR agonist [54]. EBF2 also induces the expression of brown-adipocyte–specific genes, including *Prdm16*, *Pgc1α*, *Pparα*, and *Cidea*. C/EBPβ has been reported to positively modulate EBF2 expression [55]. Our previous study demonstrated that Cryptotanshinone can induce EBF2 expression by STAT3 signalling in the early commitment of brown lineage [19]. Our findings suggest that MF promotes brown-lineage commitment by inducing early brown commitment markers EBF2 in C3H10T1/2 MSCs. Nonetheless, the precise mechanisms of action of MF in early commitment requires further research.

Although MF shows a potential anti-obesity effect by improving non-shivering thermogenesis in vitro, several challenges must be solved before MF can demonstrate a potent effect within in vivo models. Interestingly, previous studies have shown that MF-enriched plant extract prevents high fat diet (HFD)-induced obesity in several animal models including rats [56] and C57BL6/J mice [57]. Apontes and Liu et al. reported that MF treatment decreases 50% of the body weight of HFD-induced C57BL/6J mice without affecting food or water intake [52]. The MF-mediated body weight reduction was accompanied by the prevention of whole-body abdominal fat accumulation and a reduction in lean mass as an indicator of total fat mass. This study also showed that MF treatment substantially increases basal body temperature in mice maintained at an ambient or cold temperature and speculated that MF treatment increased thermogenesis in brown adipose tissue [52]. Additionally, in human trials, MF supplementation improved serum lipid profiles, shivering thermogenesis [52,58], and diabetes symptoms [59]. These studies showed that MF is orally bioavailable in rodents and humans and potentially ameliorates obesity. The role of MF in browning has not been addressed. Our study demonstrated a detailed mechanism of MF action for reduce obesity by inducing and maintaining browning. There are several chemicals such as raspberry ketone [24], liensinine [23], and CL316,243 [41] have been reported to suppress the transition from beige to white adipocytes via inhibition of mitophagy. This study suggests that MF is a notable phytochemical that can induce browning and mitophagy markers including p62 and decrease the expression of lipogenesis markers.

5. Conclusion

In summary, MF is a widely studied orally bioavailable phytochemical known to reduce obesity-related syndromes in both in vivo and clinical trials. However, its role non-shivering thermogenesis remains elusive. Thus, in our in vitro study, we reported the role of MF in browning and the related metabolic process. MF promotes the expression of brown and beige markers and inhibits the beige-to-white transition by suppressing PINK1–PRKN-mediated mitophagy by activating β3-AR–dependent PKA-p38 MAPK-CREB signalling in C3H10T1/2MSCs. Thus, MF may be a good nutritional supplement against obesity and related metabolic diseases. However, several scopes require further attention such as a ligand binding assay to establish MF as a β3-AR agonist and involvement of the CREB signalling axis. Moreover, MF administration using PINK1/PRKN-deficient mice or iWAT of mice can reveal the define mechanism of MF-mediated browning by suppressing PINK1/PRKN-mediated mitophagy, which can expand our in vitro findings to the same in the clinical setting.

Supplementary data to this article can be found online at https://doi.org/10.1016/j.metabol.2020.154228.

CRediT authorship contribution statement

Md. Shamim Rahman: Methodology, Formal analysis, Investigation, Writing - original draft. **Yong-Sik Kim:** Methodology, Formal analysis, Writing - original draft.

Acknowledgements

This research was supported by the Basic Science Research Program through the National Research Foundation of Korea (NRF) funded by the Ministry of Education (2015R1A6A103032522; 2017R1D1A1B03032455) and partially by a research fund of Soonchunhyang University.

Declaration of competing interest

The authors declare that they have no conflicts of interest.

References

[1] Bhupathiraju SN, Hu FB. Epidemiology of obesity and diabetes and their cardiovascular complications. Circ Res 2016;118:1723–35.
[2] Harms M, Seale P. Brown and beige fat: development, function and therapeutic potential. Nat Med 2013;19:1252–63.
[3] Ikeda K, Maretich P, Kajimura S. The common and distinct features of brown and beige adipocytes. Trends Endocrinol Metab 2018;29:191–200.
[4] Sidossis L, Kajimura S. Brown and beige fat in humans: thermogenic adipocytes that control energy and glucose homeostasis. J Clin Invest 2015;125:478–86.
[5] Um JH, Yun J. Emerging role of mitophagy in human diseases and physiology. BMB Rep 2017;50:299–307.
[6] Shiau M-Y, Lee P-S, Huang Y-J, Yang C-P, Hsiao C-W, Chang K-Y, et al. Role of PARL-PINK1-Parkin pathway in adipocyte differentiation. Metab Clin Exper 2017;72:1–17.
[7] Rodger CE, McWilliams TG, Ganley IG. Mammalian mitophagy — from in vitro molecules to in vivo models. FEBS J 2018;285:1185–202.
[8] Narendra DP, Jin SM, Tanaka A, Suen D-F, Gautier CA, Shen J, et al. PINK1 is selectively stabilized on impaired mitochondria to activate Parkin. PLoS Biol 2010;8:e1000298.
[9] Matsuda N, Sato S, Shiba K, Okatsu K, Saisho K, Gautier CA, et al. PINK1 stabilized by mitochondrial depolarization recruits Parkin to damaged mitochondria and activates latent Parkin for mitophagy. J Cell Biol 2010;189:211–21.
[10] Lazarou M, Sliter DA, Kane LA, Sarraf SA, Wang C, Burman JL, et al. The ubiquitin kinase PINK1 recruits autophagy receptors to induce mitophagy. Nature 2015;524:309–14.

[11] Heo J-M, Ordureau A, Paulo JA, Rinehart J, Harper JW. The PINK1-PARKIN mitochondrial ubiquitylation pathway drives a program of OPTN/NDP52 recruitment and TBK1 activation to promote mitophagy. Mol Cell 2015;60:7–20.
[12] Murakawa T, Yamaguchi O, Hashimoto A, Hikoso S, Takeda T, Oka T, et al. Bcl-2-like protein 13 is a mammalian Atg32 homologue that mediates mitophagy and mitochondrial fragmentation. Nat Commun 2015;6:7527.
[13] Wrighton KH. Mitophagy turns beige adipocytes white. Nat Rev Mol Cell Biol 2016;17:607.
[14] Altshuler-Keylin S, Shinoda K, Hasegawa Y, Ikeda K, Hong H, Kang Q, et al. Beige adipocyte maintenance is regulated by autophagy-induced mitochondrial clearance. Cell Metab 2016;24:402–19.
[15] Lu X, Altshuler-Keylin S, Wang Q, Chen Y, Henrique Sponton C, Ikeda K, et al. Mitophagy controls beige adipocyte maintenance through a Parkin-dependent and UCP1-independent mechanism. Sci Signal 2018;11.
[16] Sarraf SA, Youle RJ. Parkin mediates mitophagy during beige-to-white fat conversion. Sci Signal 2018;11.
[17] Chen J, Ren Y, Gui C, Zhao M, Wu X, Mao K, et al. Phosphorylation of Parkin at serine 131 by p38 MAPK promotes mitochondrial dysfunction and neuronal death in mutant A53T alpha-synuclein model of Parkinson's disease. Cell Death Dis 2018;9:700.
[18] Kim D, Kim JH, Kang YH, Kim JS, Yun SC, Kang SW, et al. Suppression of brown adipocyte autophagy improves energy metabolism by regulating mitochondrial turnover. Int J Mol Sci 2019;20.
[19] Imran KM, Rahman N, Yoon D, Jeon M, Lee BT, Kim YS. Cryptotanshinone promotes commitment to the brown adipocyte lineage and mitochondrial biogenesis in C3H10T1/2 mesenchymal stem cells via AMPK and p38-MAPK signaling. Biochim Biophys Acta Mol Cell Biol Lipids 1862;2017:1110–20.
[20] Wang X, Chen J, Rong C, Pan F, Zhao X, Hu Y. GLP-1RA promotes brown adipogenesis of C3H10T1/2 mesenchymal stem cells via the PI3K-AKT-mTOR signaling pathway. Biochem Biophys Res Commun 2018;506:976–82.
[21] Zhang Z, Zhang H, Li B, Meng X, Wang J, Zhang Y, et al. Berberine activates thermogenesis in white and brown adipose tissue. Nat Commun 2014;5:5493.
[22] Wang H, Mao X, Du M. Phytanic acid activates PPARalpha to promote beige adipogenic differentiation of preadipocytes. J Nutr Biochem 2019;67:201–11.
[23] Xie S, Li Y, Teng W, Du M, Li Y, Sun B. Liensinine inhibits beige adipocytes recovering to white adipocytes through blocking mitophagy flux in vitro and in vivo. Nutrients 2019;11.
[24] Leu SY, Tsai YC, Chen WC, Hsu CH, Lee YM, Cheng PY. Raspberry ketone induces brown-like adipocyte formation through suppression of autophagy in adipocytes and adipose tissue. J Nutr Biochem 2018;56:116–25.
[25] Du M, Wen G, Jin J, Chen Y, Cao J, Xu A. Mangiferin prevents the growth of gastric carcinoma by blocking the PI3K-Akt signalling pathway. Anticancer Drugs 2017;29(2):167–75.
[26] Sekar V, Mani S, Malarvizhi R, Nithya P, Vasanthi HR. Antidiabetic effect of mangiferin in combination with oral hypoglycemic agents metformin and gliclazide. Phytomedicine 2019;59:152901.
[27] Ramirez NM, Toledo RCL, Moreira MEC, Martino HSD, Benjamin LDA, de Queiroz JH, et al. Anti-obesity effects of tea from Mangifera indica L. leaves of the Uba variety in high-fat diet-induced obese rats. Biomed Pharmacother 2017;91:938–45.
[28] Sim MO, Lee HJ, Jeong DE, Jang JH, Jung HK, Cho HW. 6'-O-acetyl mangiferin from Iris rossii Baker inhibits lipid accumulation partly via AMPK activation in adipogenesis. Chem Biol Interact 2019;311:108755.
[29] Subash-Babu P, Alshatwi AA. Evaluation of antiobesity effect of mangiferin in adipogenesis-induced human mesenchymal stem cells by assessing adipogenic genes. J Food Biochem 2015;39:28–38.
[30] Schild L, Dombrowski F, Lendeckel U, Schulz C, Gardemann A, Keilhoff G. Impairment of endothelial nitric oxide synthase causes abnormal fat and glycogen deposition in liver. Biochim Biophys Acta (BBA) Mol Basis Dis 2008;1782:180–7.
[31] Strappazzon F, Nazio F, Corrado M, Cianfanelli V, Romagnoli A, Fimia GM, et al. AMBRA1 is able to induce mitophagy via LC3 binding, regardless of PARKIN and p62/SQSTM1. Cell Death Differ 2015;22:419–32.
[32] Koh YJ, Park B-H, Park J-H, Han J, Lee I-K, Park JW, et al. Activation of PPARγ induces profound multilocularization of adipocytes in adult mouse white adipose tissues. Exp Mol Med 2009;41:880–95.
[33] Jahagirdar A, Usharani D, Srinivasan M, Rajasekharan R. Sesaminol diglucoside, a water-soluble lignan from sesame seeds induces brown fat thermogenesis in mice. Biochem Biophys Res Commun 2018;507:155–60.
[34] Gomes LC, Di Benedetto G, Scorrano L. During autophagy mitochondria elongate, are spared from degradation and sustain cell viability. Nat Cell Biol 2011;13:589–98.
[35] Toyama EQ, Herzig S, Courchet J, Lewis Jr TL, Losón OC, Hellberg K, et al. Metabolism. AMP-activated protein kinase mediates mitochondrial fission in response to energy stress. Science (New York, NY) 2016;351:275–81.
[36] Kang SWS, Haydar G, Taniane C, Farrell G, Arias IM, Lippincott-Schwartz J, et al. AMPK activation prevents and reverses drug-induced mitochondrial and hepatocyte injury by promoting mitochondrial fusion and function. PloS One 2016;11 e0165638-e.
[37] Pisani DF, Barquissau V, Chambard JC, Beuzelin D, Ghandour RA, Giroud M, et al. Mitochondrial fission is associated with UCP1 activity in human brite/beige adipocytes. Mol Metab 2018;7:35–44.
[38] Cao W, Medvedev AV, Daniel KW, Collins S. beta-Adrenergic activation of p38 MAP kinase in adipocytes: cAMP induction of the uncoupling protein 1 (UCP1) gene requires p38 MAP kinase. J Biol Chem 2001;276:27077–82.
[39] McWilliams TG, Prescott AR, Montava-Garriga L, Ball G, Singh F, Barini E, et al. Basal mitophagy occurs independently of PINK1 in mouse tissues of high metabolic demand. Cell Metab 2018;27:439–49 e5.
[40] Cairo M, Villarroya J. The role of autophagy in brown and beige adipose tissue plasticity. J Physiol Biochem 2019. https://doi.org/10.1007/s13105-019-00708-1.
[41] Taylor D, Gottlieb RA. Parkin-mediated mitophagy is downregulated in browning of white adipose tissue. Obesity (Silver Spring) 2017;25:704–12.
[42] Lu Y, Fujioka H, Joshi D, Li Q, Sangwung P, Hsieh P, et al. Mitophagy is required for brown adipose tissue mitochondrial homeostasis during cold challenge. Sci Rep 2018;8:8251.
[43] Martinez-Lopez N, Athonvarangkul D, Sahu S, Coletto L, Zong H, Bastie CC, et al. Autophagy in Myf5+ progenitors regulates energy and glucose homeostasis through control of brown fat and skeletal muscle development. EMBO Rep 2013;14:795–803.
[44] Cairo M, Campderros L, Gavalda-Navarro A, Cereijo R, Delgado-Angles A, Quesada-Lopez T, et al. Parkin controls brown adipose tissue plasticity in response to adaptive thermogenesis. EMBO Rep 2019;20.
[45] Muller TD, Lee SJ, Jastroch M, Kabra D, Stemmer K, Aichler M, et al. p62 links beta-adrenergic input to mitochondrial function and thermogenesis. J Clin Invest 2013;123:469–78.
[46] Cairo M, Villarroya J, Cereijo R, Campderros L, Giralt M, Villarroya F. Thermogenic activation represses autophagy in brown adipose tissue. Int J Obes (Lond) 2016;40:1591–9.
[47] Liu Z, Apontes P, Fomenko EV, Chi N, Schuster VL, Kurland IJ, et al. Mangiferin accelerates glycolysis and enhances mitochondrial bioenergetics. Int J Mol Sci 2018;19.
[48] Huang TH, Peng G, Li GQ, Yamahara J, Roufogalis BD, Li Y. Salacia oblonga root improves postprandial hyperlipidemia and hepatic steatosis in Zucker diabetic fatty rats: activation of PPAR-alpha. Toxicol Appl Pharmacol 2006;210:225–35.
[49] Lim J, Liu Z, Apontes P, Feng D, Pessin JE, Sauve AA, et al. Dual mode action of mangiferin in mouse liver under high fat diet. PLoS One 2014;9:e90137.
[50] Flachs P, Horakova O, Brauner P, Rossmeisl M, Pecina P, Franssen-van Hal N, et al. Polyunsaturated fatty acids of marine origin upregulate mitochondrial biogenesis and induce beta-oxidation in white fat. Diabetologia 2005;48:2365–75.
[51] Lim SC, Tajika M, Shimura M, Carey KT, Stroud DA, Murayama K, et al. Loss of the mitochondrial fatty acid beta-oxidation protein medium-chain acyl-coenzyme A dehydrogenase disrupts oxidative phosphorylation protein complex stability and function. Sci Rep 2018;8:153.
[52] Apontes P, Liu Z, Su K, Benard O, Youn DY, Li X, et al. Mangiferin stimulates carbohydrate oxidation and protects against metabolic disorders induced by high-fat diets. Diabetes 2014;63:3626–36.
[53] Pardo-Andreu GL, Paim BA, Castilho RF, Velho JA, Delgado R, Vercesi AE, et al. Mangifera indica L. extract (Vimang) and its main polyphenol mangiferin prevent mitochondrial oxidative stress in atherosclerosis-prone hypercholesterolemic mouse. Pharmacol Res 2008;57:332–8.
[54] Stine RR, Shapira SN, Lim HW, Ishibashi J, Harms M, Won KJ, et al. EBF2 promotes the recruitment of beige adipocytes in white adipose tissue. Mol Metab 2016;5:57–65.
[55] Jimenez MA, Akerblad P, Sigvardsson M, Rosen ED. Critical role for Ebf1 and Ebf2 in the adipogenic transcriptional cascade. Mol Cell Biol 2007;27:743–57.
[56] Yoshikawa M, Shimoda H, Nishida N, Takada M, Matsuda H. Salacia reticulata and its polyphenolic constituents with lipase inhibitory and lipolytic activities have mild antiobesity effects in rats. J Nutr 2002;132:1819–24.
[57] Im R, Mano H, Nakatani S, Shimizu J, Wada M. Aqueous extract of Kotahla Himbutu (Salacia reticulata) stems promotes oxygen consumption and supresses body fat accumulation in mice. J Health Sci 2008;54:645–53.
[58] Gelabert-Rebato M, Wiebe JC, Martin-Rincon M, Galvan-Alvarez V, Curtelin D, Perez-Valera M, et al. Enhancement of exercise performance by 48 hours, and 15-day supplementation with mangiferin and luteolin in men. Nutrients 2019;11.
[59] Kitalong C, Nogueira RC, Benichou J, Yano V, Espangel V, Houriet J, et al. "DAK", a traditional decoction in Palau, as adjuvant for patients with insufficient control of diabetes mellitus type II. J Ethnopharmacol 2017;205:116–22.